Solvation structure and dynamics of Li and LiO_2 and their transformation in non-aqueous organic electrolyte solvents from first-principles simulations

Behnaz Rahmani Didar[a], Axel Groß[a,b,*]

[a] *Institute of Theoretical Chemistry, Ulm University, Albert-Einstein-Allee 11, D-89081 Ulm, Germany*
[b] *Helmholtz Institute Ulm (HIU) Electrochemical Energy Storage, Helmholtzstrasse 11 D-89081 Ulm, Germany*

Abstract

Density functional theory calculations together with ab initio molecular dynamics (AIMD) simulations have been used to study the solvation, diffusion and transformation of Li^+ and LiO_2 upon O_2 reduction in three organic electrolytes. These processes are critical for the performance of Li-air batteries. Apart from studying the structure of the solvation shells in detail, AIMD simulations have been used to derive the diffusivity and together with the Blue Moon ensemble approach to explore LiO_2 formation from Li^+ and O_2^- and the subsequent disproportionation of $2LiO_2$ into Li_2O_2 + O_2. By comparing the results of the simulations to gas phase calculations the impact of electrolytes on these reactions is assessed which turns out to be more pronounced for the ionic species involved in these reactions.

Keywords: Li-air batteries, Li oxide, oxygen reduction, density functional theory, ab initio molecular dynamics

1. Introduction

Li-air batteries have shown theoretical energy densities far greater than that of Li-ion batteries, making these contender batteries a promising candidate for

*Corresponding author
Email address: axel.gross@uni-ulm.de (Axel Groß)

electric vehicles and large scale energy storage stations [1, 2, 3, 4, 5, 6]. In the operation of a Li-air battery in non-aqueous aprotic solvents, O_2 reduction which is one of the most studied reactions in chemistry [7, 8] is of central importance. In general, upon discharge Li^+ from the anode reacts with oxygen anions (O_2^- and O_2^{2-}) that are formed at the cathode through reduction of O_2 from the gas phase, leading to LiO_2 (intermediate product), Li_2O (discharge product) and Li_2O_2 (main discharge product). Spectroscopic studies of O_2 reduction in an aprotic solvent specifically suggest that LiO_2 is first formed as an intermediate which then further disproportionates to Li_2O_2 [7]. This means that the formation of Li_2O_2 does not proceed via the direct two-electron electroreduction of O_2 to O_2^{2-}, which is the common O_2 reduction pathway in water, but rather as a one–electron reduction to O_2^- followed by a disproportionation reaction.

Ideally, during recharge associated with oxygen evolution, these products are brought back to their initial forms of Li and molecular oxygen. However, practically achieving the theoretically promised high energy density and maintaining rechargeability and high cyclability has posed a major challenge in the commercialization of Li-air batteries [9]. Instability and decomposition of the electrolyte, and deposition of the electrically-insulating main discharge product (Li_2O_2) on the cathode and its pore clogging effects, have been identified as the main causes of this problem [1, 2, 10, 11, 12, 13, 14, 15, 16].

Although several theoretical studies have shown that the top layers of Li_2O_2 are in fact metallic and may provide conducting pathways [17, 18, 19, 20], growth of Li_2O_2 particles in the solution phase rather than its deposition on the cathode is proposed to be more advantageous to the cycling capability of the cell [13, 16]. Decomposition and degradation of the electrolyte has been observed mostly with the use of carbonate based electrolytes where little or no Li_2O_2 is formed during discharge [2] to be reversed back to Li during recharge. In contrast, organic non-carbonate solvents such as dimethoxyethane (DME) (ether), dimethyl sulfoxide (DMSO), and acetonitrile (ACN), have shown a higher stability in the presence of reduced O_2 species [2]. Studies have shown that the stability of intermediate products (LiO_2 and O anions), may strongly depend on the donor/acceptor

number (donicity) of the solvent [21, 22, 9, 23]. High donor number solvents such as DMSO (which has oxygen lone pairs) can solvate Li^+ and Li^+-containing species and give rise to superoxide (O_2^- or LiO_2) in the solution [24, 25, 26, 27]. In fact, solvent donicity has been linked to the O_2 reduction pathway to form Li_2O_2, through the solubility of LiO_2 and the free energy of $LiO_2 \rightarrow Li + O_2$ [26, 9, 27]. It is argued that with low donicity solvents, Li^+ is weakly solvated which leads to surface-adsorbed LiO_2 and eventually Li_2O_2 films being formed near the electrode [26, 9, 25].

Therefore, it is clear that solubility and diffusion of Li^+, oxygen anions, and LiO_2 in the electrolyte solvent are critical parameters that affect reaction mechanisms and the overall function of Li-air cells. Studies on the oxygen reduction reaction and oxygen anion species are well-documented [22, 9, 24, 23, 28, 25]. Still, some fundamental properties of Li^+ and LiO_2 including solvation structure and shell, energetics, dynamics, transport properties and molecular mechanisms have not been explored in detail. These properties and the interplay between them play a key role in the reaction mechanisms and the overall function of Li-air cells.

First-principles methods such as density functional theory (DFT) and *ab initio* molecular dynamics (AIMD), are based on quantum mechanics principles. These class of simulations can provide valuable information regarding solvation and dynamics of species in the cell, and therefore guide the design of battery materials [29]. The papers of Das et al. [30], Ong et al. [31], Pham et al. [32], and Chaudhari et al. [33] present a few examples of studies that have used first-principles methods to investigate the stability of discharge products and solvation and diffusion in electrolytes of Li-air and Li-ion batteries. Bryantsev et al. used DFT to address the stability of LiO_2 and the free energy pathway to Li_2O_2 formation in Li-air batteries [34]. Still, these calculations have all been performed in the gas phase and in the absence of any electrolyte. Their study demonstrated that there is a strong thermodynamic driving force for the formation of Li_2O_2 from LiO_2. Furthermore, many studies have focused on the generation and growth of the discharge products directly on the electrode

surface [35, 36, 37], however, to the best of our knowledge, studies addressing lithium peroxide formation in solution are scarce.

In this work, we focus on non-electrochemical processes and use DFT and AIMD to study the solvation and diffusion of Li^+ and LiO_2 in the three organic electrolytes DME, DMSO and ACN. In addition, we use the Blue Moon Ensemble and constrained molecular dynamics to explore LiO_2 dissociation ($LiO_2 \rightarrow Li + O_2$) and disproportionation ($2LiO_2 \rightarrow Li_2O_2 + O_2$) reactions in three electrolytes. In particular, we will show that both reactions should occur spontaneously in all considered electrolytes, but we will identify characteristic differences in the performance of these three electrolytes.

2. Calculational details

Spin-polarized periodic DFT calculations were performed using the Vienna ab initio simulation package (VASP) [38] with the projected augmented wave (PAW) method [39, 40]. Exchange-correlation effects were considered within the generalized gradient approximation (GGA) using the Perdew-Burke-Ernzerhof (PBE) functional [41] and its revised version (RPBE) [42]. The wave functions were expanded in a plane wave basis with a kinetic cut-off energy of 400 eV. Dispersion effects were taken into account within the DFT-D3 method [43]. In particular the RPBE-D3 approach has been shown to yield reliable solvation structures [44, 45] and interaction energies [46]. A convergence criterion with an energy of 10^{-6} eV was used for all calculations.

Three different electrolytes were studied; DME, DMSO, and ACN. The simulation boxes chosen for these three different electrolytes had the size 12Å $\times$ 12Å $\times$ 12Å. To ensure charge neutrality, Li^+ was considered together with its counter ion ($Li^+PF_6{}^-$) commonly used as salt in Li-based batteries. For each of theses systems, a $LiPF_6$ was first placed in the simulation box, with the remaining free volume of the box packed with enough electrolyte yielding its certain density (DME: 0.87 g cm^{-3}, DMSO: 1.1 g cm^{-3}, ACN: 0.79 g cm^{-3}) and ion (or salt) concentration of 1 M. Then, geometry optimization was performed on

each configuration with classical molecular mechanics using the universal force field.

These relaxed structures were used for subsequent *ab initio* molecular dynamics simulations (AIMD) simulations. AIMD simulations were performed in the NVT ensemble using a Nosé-Hoover thermostat [47, 48] with a time step of 0.5 fs. All systems were first equilibrated for 5 ps and then simulated for 25 ps to gather statistics. A temperature of 300 K was used, dictated by normal battery operating conditions. Pair correlation functions were used to characterize solvation structures. The integral of the pair correlation function was used to calculate coordination numbers for each system.

Interaction energies between a single species X and Y in the gas phase were calculated according to

$$E_{\mathrm{int}} = E_{\mathrm{XY}} - E_{\mathrm{X}} - E_{\mathrm{Y}} \ , \tag{1}$$

where E_{XY}, E_{X}, and E_{Y} are the total energies of XY, X, and Y in the gas phase, respectively. A large number of possible configurations of the species were tested and optimized. Those reported belong to the most favorable configurations. Bond lengths were extracted from optimized force field structures.

In order to illustrate the charge rearrangement and thus the nature of the interaction [49] between ions and the solvent molecules, we have determined charge density differences

$$\Delta\rho = \rho_{\mathrm{total}} - \rho_{\mathrm{ion}} - \rho_{\mathrm{solventmolecule}} \ , \tag{2}$$

where ρ_{total}, ρ_{ion}, and $\rho_{\mathrm{solventmolecule}}$ are the total charge density of the system, charge density of the ion (e.g. Li), and charge density of the solvent molecule (e.g. DME molecule), respectively. In order to illustrate areas of electron accumulation and depletion, we have determined charge difference isosurfaces at a density of ± 0.005 e$\mathrm{\AA}^{-3}$.

We estimated the solvation energy (ΔE_{sol}) of Li^+ in different electrolytes based on cluster calculations by

$$\Delta E_{\mathrm{sol}} = E_{\mathrm{Li}^+,(\mathrm{solvent})_n} - E_{\mathrm{Li}^+} - E_{(\mathrm{solvent})_n} \ , \tag{3}$$

as done previously [32], where $E_{\mathrm{Li^+,(solvent)}_n}$, $E_{\mathrm{Li^+}}$, and $E_{\mathrm{(solvent)}_n}$ are the total energy of the cluster of Li^+ and the electrolyte molecules in the first solvation shell, total energy of Li^+, and total energy of the electrolyte molecules in the first solvation shell, respectively. The clusters were extracted directly from AIMD simulations and therefore implicitly include temperature and dynamic effects. The solvation energy of LiO_2 in the electrolytes was estimated by the same approach, but with LiO_2 substituted for Li^+.

Diffusion coefficients were calculated from the linear regression of the mean square displacement (MSD) over time using the Stokes-Einstein equation [50]:

$$D = \frac{1}{6}\frac{<(\Delta r)^2>}{\Delta t} \tag{4}$$

The MSD was calculated by averaging over multiple trajectory windows spanning the entire trajectory, using window lengths of 5 ps in increments of 1 ps. The slope of the linear section of the MSD vs time was used to calculate D from Eq. 4 for each system.

Here we used the thermodynamic integration slow growth approach to obtain free energy profiles of the reactions of interest [51, 52]. This AIMD method has been implemented in VASP as the Blue Moon ensemble method [53, 54, 55]. Starting from an initial optimized structure and an initial location (ξ_1) the motion is followed along the reaction coordinate (collective variable) to a final defined location (ξ_2), while the free energy gradient ($\delta F/\Delta\xi$) is collected along this path. We used a step size of 0.00008 Å for every femtosecond, with which to collect free energy gradients. We averaged the dynamic trajectories over every 1000 steps. The free energy (ΔF) profile was then obtained by integrating over the $\xi_1 \rightarrow \xi_2$ path.

3. Results and Discussion

3.1. Interaction Energies

As a first step, we have carried out an in depth study of interaction energetics and structure of Li and LiO_2 in the three considered electrolytes. Table 1

shows the interaction energies according to Eq. 1, determined using the PBE and RPBE functionals without and with D3 dispersion corrections, of a single Li atom and a LiO_2 molecule with each of the three different electrolyte molecules. The optimized structures are shown in the Supporting Information. The trends among the different functionals are similar to those found before [44, 46, 56]. In general, RPBE yields a slightly lower interaction strength than PBE. For both functionals, dispersion corrections lead to stronger interactions as expected upon adding an attractive interaction. However, the differences are rather small. In the following, we will use the RPBE-D3 functional for the AIMD simulations.

According to our calculations, Li atom prefers to bond to the N atom of the ACN molecule, and the O atom of both DMSO and DME molecules. Table 1 demonstrates that the order of the interaction strength between an Li atom and an electrolyte molecule is DME $>$ DMSO $>$ ACN across all considered functionals. The same order in the interaction strength is also obtained for the LiO_2 interaction with the three different electrolyte molecules. In spite of the strongest interaction, DME exhibits also the longest bond length with the Li atom, as listed in Tab. 2. This is closely followed by Li-ACN, and lastly Li-DMSO. The same trend is observed for the calculated bond length between LiO_2 and each of the three electrolyte molecules.

Table 1: Interaction energies (in eV) of Li and LiO_2 with electrolyte molecules obtained from DFT calculations using Eq. 1.

		PBE	PBE-D3	RPBE	RPBE-D3
Li					
	ACN (Li-N)	-0.50	-0.52	-0.47	-0.49
	DMSO (Li-O)	-0.76	-0.79	-0.67	-0.72
	DME (Li-O)	-0.82	-0.83	-0.70	-0.80
LiO_2					
	ACN (Li-N)	-0.84	-0.88	-0.81	-0.86
	DMSO (Li-O)	-0.98	-1.01	-0.94	-1.00
	DME (Li-O)	-1.05	-1.06	-0.95	-1.14

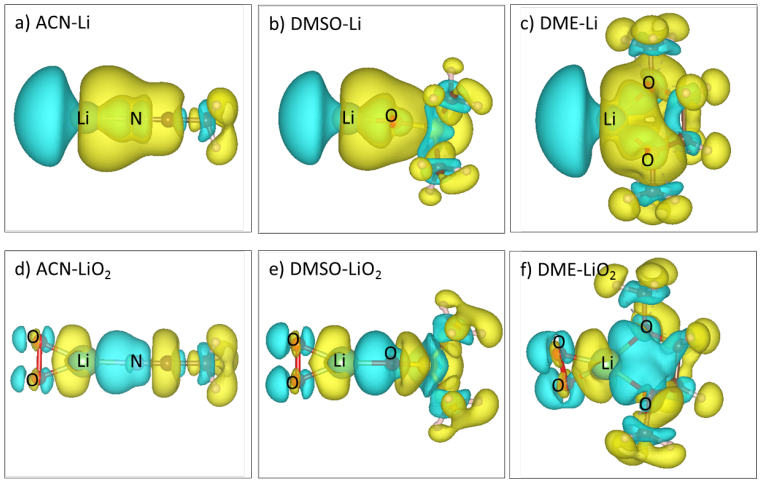

Figure 1: Charge density difference $\Delta\rho$ upon the interaction of Li with a) ACN, b) DMSO and c) DME molecules, and LiO_2 with d) ACN, e) DMSO and f) DME molecules, as obtained from DFT calculations using Eq. 2. Cyan and yellow regions correspond to electron accumulation and depletion, respectively. The isosurface levels are ± 0.005 eV Å^{-3}.

The special role of DME can easily be understood by the fact that it interacts with the Li atom through the bonding to two oxygen atoms in a bidentate fashion, which can also be seen in the charge density difference plots shown in Fig. 1. Interestingly enough, these plots also illustrate that in the case of the single Li atom interacting with the electrolyte molecules, there is a charge depletion at the O and the N atoms, with some charge transfer towards the Li atom, whereas in the case of LiO_2 there is a charge accumulation close to the O and the N atoms and a more complex polarization pattern within the whole complex.

3.2. First Solvation Shell Structures

We now turn to an analysis of the AIMD runs. Note that, for the solvation of Li^+, we performed two independent simulations for each electrolyte with one Li^+-PF_6^- pair in the simulation box, where the Li^+-PF_6^- ion pair was either initially associated or dissociated. For the case of ACN as the electrolyte, the initially associated $LiPF_6$, dissociated within the first 2ps and remained so for

Table 2: Bond lengths in Å for the interactions of Li and LiO_2 with electrolyte molecules obtained from DFT calculations.

		PBE	PBE-D3	RPBE	RPBE-D3
Li					
	ACN (Li-N)	1.94	1.94	1.99	2.00
	DMSO (Li-O)	1.80	1.80	1.85	1.82
	DME (Li-O)	1.98	1.99	2.00	2.04
LiO_2					
	(ACN)				
	Li-N	2.07	2.04	2.16	2.05
	Li-O	1.82	1.81	1.83	1.83
	O-O	1.36	1.37	1.37	1.37
	(DMSO)				
	Li-O	1.88	1.90	1.92	1.91
	Li-O	1.81	1.82	1.83	1.83
	Li-O	1.37	1.37	1.37	1.37
	(DME)				
	Li-O	2.06	2.16	2.12	2.09
	Li-O	1.83	1.83	1.84	1.83
	Li-O	1.37	1.37	1.37	1.38

the remainder of the time. The initially dissociated $LiPF_6$ remained dissociated for the entire simulation run time of 30ps. For the case of DMSO as the electrolyte, both the associated and dissociated $LiPF_6$ ion pair remained so for the duration of the simulations. In terms of thermodynamic stability, the associated $LiPF_6$ structure was more favorable than the dissociated, as indicated by the lower DFT total energy along the AIMD runs. Similarly, for the case of DME as the electrolyte, both the associated and dissociated $LiPF_6$ ion pair also remained so for the duration of the simulations and the associated structure was more energetically favorable than the dissociated.

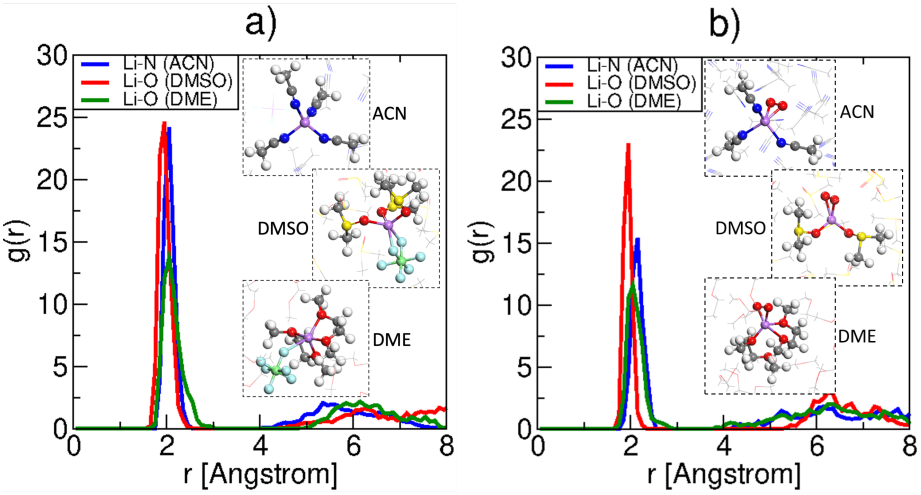

Figure 2: Radial distribution functions of the Li-O and Li-N distances, respectively, obtained from AIMD simulations of a) Li and b) LiO_2 in 1 M ACN, DMSO and DME electrolytes. Insets show the first solvation shells for each case.

Figure 2a shows the radial distribution functions (RDF) of Li^+ with the three electrolytes (Li-N for ACN and Li-O for both DMSO and DME). At first glance, all three solvents show sharp first solvation shell peaks and clear coordination numbers in the first solvation shell. The integrated RDF, from which we can deduce coordination numbers, can be found in the Supporting Information (Figs. S1 and S2). For Li^+ in each of ACN (Li-N pair correlation function), DMSO (Li-O_{DMSO} pair correlation function) and DME (Li-O_{DME} pair correlation function), a sharp peak is seen at 2.06 , 1.97 , and 2.06 , respectively. The integrated RDFs show that Li in ACN, DMSO, and DME is bonded to 4, 3 and 2 electrolyte molecules, respectively, in the first solvation shell. Snapshots of the solvation structures (first solvation shells) are seen in insets of Figure 2. As can be seen from the insets, Li^+ in both DMSO and DME remains associated with PF_6^-. This association, and the large size of DMSO and more so DME prevent the Li^+ from bonding to more solvent molecules. Our simulations also show that Li^+ has a tetrahedral coordination geometry in the bulk ACN electrolyte solution, whereas Li^+ in bulk DMSO exhibits an undefined structure

most closely resembling that of a tetrahedron with one of the vertex corners consisting of the PF_6 bonded with two F atoms to the Li^+. Finally, Li^+ in the bulk of DME is bonded to PF_6 and four O atoms belonging to 2 DME molecules, exhibiting an intermediate geometry between a trigonal bipyramidal and s square pyramidal arrangement. Note that the PF_6 counterion did not solvate in ACN, and was only weakly bonded to solvated Li^+ in DMSO and DME.

Figure 2b depicts the radial distribution functions of LiO_2 with the three electrolytes, again with respect to the Li-N distances for ACN and Li-O distances for both DMSO and DME. The peaks of the first solvation shell are located at 2.19 , 1.97 , and 2.06 Å for LiO_2 in ACN, DMSO and DME, respectively. The integrated RDFs show that LiO_2 is bonded to 3 ACN, 2 DMSO and 2 DME molecules (with 3 O atoms) molecules, respectively, in the first solvation shell. The structure of the first solvation shell of LiO_2 in ACN appears to be a tetrahedral, similar to the first solvation shell of LiO_2 in DME although its structure is less defined. In contrast, the first solvation shell of LiO_2 in DMSO acquires a trigonal planar structure.

3.3. Solvation Energy

The magnitude of solvation energy is a good criterion for the interaction strength of the Li ion and LiO_2 with the electrolytes. Figure 3a shows the solvation energy of Li^+ in 1 M ACN, DMSO and DME solutions, measured throughout the duration of the simulations, along with the average for each electrolyte. We note that in the solvation energy calculation for Li^+ in DMSO and DME, we have taken into account the association of Li^+ with the counterion PF_6 that occurs in these two electrolytes. The solvation energy of Li^+ in DMSO and DME is similar, and considerably larger and more favorable than in ACN, suggesting that Li^+ is more tightly solvated by these larger molecules, in spite of the lower coordination. This agrees with findings from other molecular dynamics studies [57, 58].

Figure 3b depicts the solvation energy of LiO_2 in 1 M of each of the three

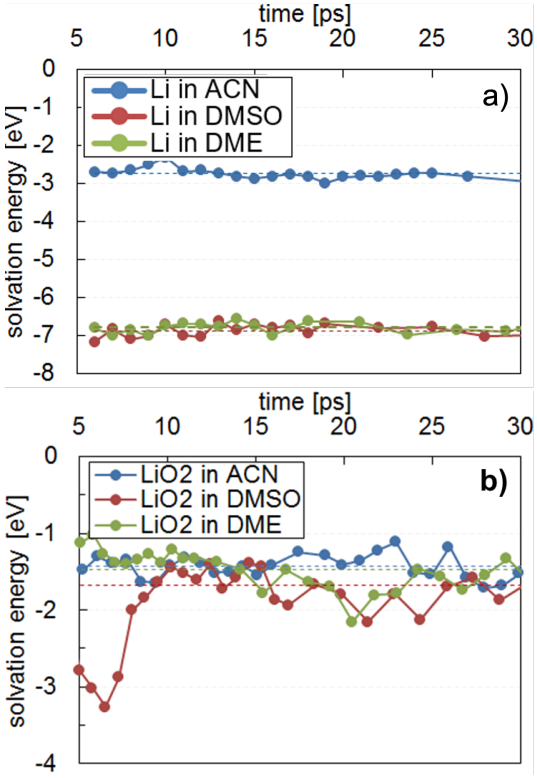

Figure 3: Solvation energies obtained from AIMD simulations of a) Li and b)LiO_2 in 1 M of each of ACN, DMSO and DME electrolytes.

electrolyte solutions, along with the average for each electrolyte. The sharp dip seen for LiO_2 solvation energy in DMSO early on in the simulation (5 ps $<$ time $<$ 10 ps) corresponds to the Li^+ instantaneously bonding to several more DMSO molecules. These bonds were then broken and remained so for the rest of the simulation time. Overall, unlike Li^+ solvation energy trends, the solvation energy of LiO_2 in all three electrolytes is quite similar to one another, although, DMSO shows slightly more favorable solvation energy towards LiO_2. This is followed by DME and ACN. Comparing the trends of solvation energy of Li^+ and LiO_2 in the three electrolytes, it is apparent that the solvation of Li^+ is more dependent upon the electrolyte.

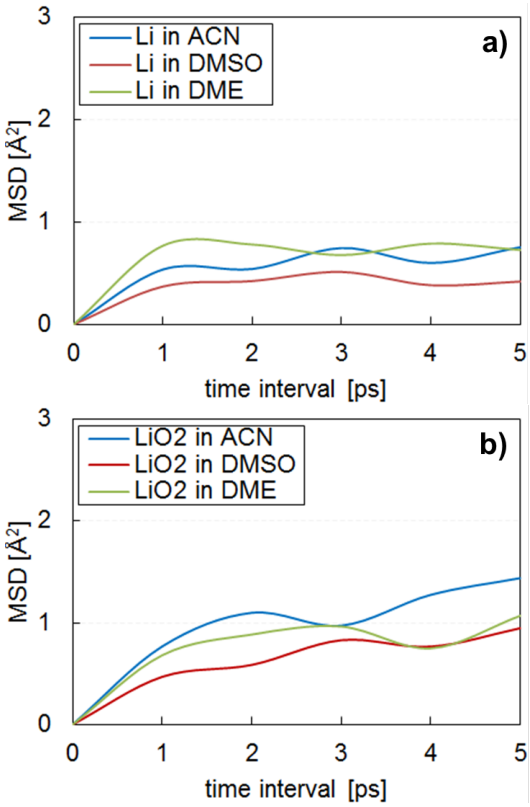

Figure 4: Diffusion obtained from AIMD simulations of a) Li and b) LiO_2 in 1 M of each of ACN, DMSO and DME electrolytes.

3.4. Diffusion

The electrolyte provides the medium through which ions present in the battery migrate and reach the electrodes. In fact, the ion mobility in the electrolyte can be a critical factor in the performance of a battery [59]. The solvation strength of ions such as Li^+ and LiO_2 in the three electrolytes studied here may influence their transportation in the electrolyte. This was investigated by means of determining the mean square distance traveled by Li^+ and LiO_2 over time, as shown in Fig. 4. Overall, the diffusion coefficients of either of Li^+ and LiO_2 are by about two to three orders of magnitude lower in the three electrolytes studied here than in carbonate solvents studied elsewhere [32, 31, 60]. Diffusion

coefficients derived for Li^+ in 1 M ACN, DMSO, and DME at 300K are ∼0.083 × 10^{-9} m^2/s, ∼0.009 × 10^{-9} m^2/s, and ∼0.002 × 10^{-9} m^2/s, respectively. Therefore, diffusion of Li^+, which follows the order of ACN > DME > DMSO, appears to be extremely low. Results in the previous section showed that the solvation of Li^+ was the least energetically favorable in ACN. Taken together, we conclude that Li^+ is less bound by and therefore freer to move within ACN, and that Li^+ is more tightly solvated by DMSO. Compared with Li^+, LiO_2 shows slightly larger diffusion in the three electrolytes. Diffusion coefficients derived for LiO_2 in 1 M ACN, DMSO, and DME at 300K are ∼0.25 × 10^{-9} m^2/s, ∼0.24 × 10^{-9} m^2/s, and ∼0.11 × 10^{-9} m^2/s, respectively. Therefore the diffusion coefficient follows the ACN > DME > DMSO order. These results agree well with the solvation energy trends of ACN < DME < DMSO from the previous section.

3.5. Association and Disproportionation Reactions

3.5.1. Association ($Li^+ + O_2^+ \rightarrow LiO_2$)

In this section, we will discuss the reactions occuring during discharge in a Li-air battery which provide the driving force for the operation of this type of batteries. As a first step, an oxygen superoxide anion (O_2^-) provided by the cathode reacts with the Li cation provided by the anode to form LiO_2. LiO_2 is unstable in its bulk phase at room temperature [34, 61] and is generally considered as an intermediate product. The LiO_2 stability in the dissolved form has been shown to be dependent on the electrolyte [9, 22]. Here we employed Blue Moon ensemble AIMD simulations to study the LiO_2 stability in the dissolved form by obtaining the reaction energy barrier for LiO_2 dissociation into Li^2 and O_2^- in the three electrolytes. We then reversed this path to illustrate the formation of LiO_2 from Li^2 and O_2^-. The resulting free energy profiles of this reaction (association) in the three electrolytes are shown in Fig. 5 alongside that of vacuum. Figures S3 and S4 in the Supporting Information show the results in detail for each electrolyte. LiO_2 in vacuum is 2.19 eV more stable than Li^+ and O_2^-. As for the LiO_2 stability in the electrolytes, results show that LiO_2 is

0.85 eV, 0.70 eV and 0.53 eV more stable in DME, ACN and DMSO respectively, than Li^2 and O_2^-. Thus, the resulting order of stability of LiO_2 in the three electrolytes is DME > ACN > DMSO and therefore, the association reaction is most favorable in DME among the considered electrolytes. This is in agreement with the experimental findings of Scheers *et al.*[28]. We note that these results so far show that an individual LiO_2 molecule can form instantaneously from Li^+ and O_2^- and there is a strong thermodynamic driving force to form LiO_2 in vacuum as well as in the three electrolytes studied here.

Looking at the reverse process, the results just presented above mean that the energy barrier for LiO_2 dissociation reaction to Li^+ and O_2^- in vacuum is 2.19 eV, and the presence of an electrolyte lowers this barrier considerably and thus also lowers the energy gain upon the dissociation reaction. This can be understood by considering the fact that the solvation energy of the two ions Li^+ and O_2^- is larger than the one of the neutral LiO_2 molecule, as already illustrated in Fig. 3. Still, as just mentioned above, the chosen electrolytes support the spontaneous formation of LiO_2. However, in the next section we will see how LiO_2 molecules can easily further disproportionate to Li_2O_2 species, and are therefore unstable in the bulk solvent phase, in agreement with experimental observations [7].

3.5.2. Disproportionation ($2(LiO_2) \rightarrow Li_2O_2 + O_2$)

Once LiO_2 is formed, it can associate with other LiO_2 species to form Li_2O_2 and O_2 (disproportionation). Again we employed Blue Moon ensemble AIMD simulations to find the energy barrier for this reaction in vacuum and in electrolyte, the corresponding results are illustrated in Fig. 5b. Note first, that the energetic differences between vacuum and electrolyte calculations are much smaller than for the association reaction $Li^+ + O_2^- \rightarrow LiO_2$. As such, the electrolyte obviously has a greater impact on the association reaction than on the disproportionation reaction. Consistent with the arguments given for the influence of the electrolyte on the association reaction, in the disproportionation reaction the educts and the product all correspond to neutral molecules so that

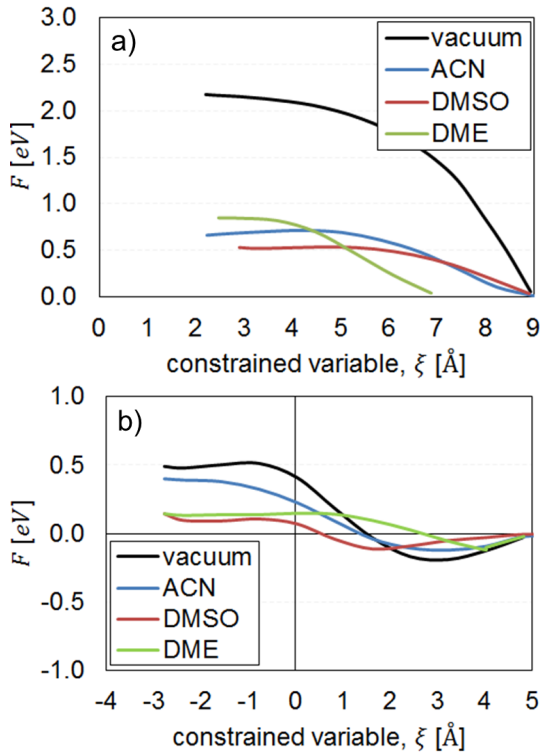

Figure 5: Reaction energy barriers obtained from the Blue Moon method of AIMD simulations for a) (Association) Li + O_2 → LiO_2) and b) (Disproportionation) 2(LiO_2) → Li_2O_2 + O_2 in vacuum and 1 M of each of ACN, DMSO and DME electrolytes.

there are no significant differences with respect to their stabilization in the presence of the solvent. Second, the results of Fig. 5b show that the formation of LiO_2 from Li_2O_2 is endothermic in all considered environments in which Li_2O_2 is obviously thermodynamically more stable than LiO_2, in agreement with the experimental results of Peng *et al.* [7] for ACN as the solvent.

Bryantsev et al [34] used DFT to study the free energy profile of this reaction in the gas phase (vacuum) by optimizing all possible intermediate structures and finding the most stable structure at each step. We note that their results using a hybrid functional with respect to the energy gain upon disproportionation in the gas phase agree rather well with our results obtained with the RPBE-D3 functional. Taking both reactions together, our calculations confirm that the

preferred pathway during discharge involves Li^+ and O_2^- atoms associating and spontaneously forming LiO_2, and the LiO_2 then further reacts to Li_2O_2. The presence of solvents reduces the thermodynamic driving force for this pathway through the stabilization of the initial ionic educts. In other words, the electrolyte helps the recharge pathway with respect to these particular steps. Still, it is important to note that the thermodynamic driving force for the overall discharge reaction $2Li+ O_2 \rightarrow Li_2O_2$ is of course not affected by the presence of the electrolyte.

Note furthermore that it is believed that insulating Li_2O_2 deposits upon discharge are supposed to be the predominant reason for the limited lifetime of Li-O_2 batteries as they can limit electron and charge transfer pathways [62, 63, 64, 18, 16]. It has been suggested that the introduction of additional cations in the electrolyte might suppress the passivation by shifting the reaction zone of Li_2O_2 formation towards the electrolyte bulk [13, 15, 17, 16] through an overcrowding of cations [65] close to the electrode. Molecular dynamics simulations show that it is possible to increase cation concentrations in the electric double layer, however, accompanying experiments indicate that the resulting drop of the Li^+ concentration close to the electrode is still not sufficient to suppress the electrode surface passivation by Li_2O_2 growth [16]. This issue will need further attention.

4. Conclusions

The properties of Li^+ and LiO_2 solvated in the three organic electrolytes dimethoxyethane (DME) (ether), dimethyl sulfoxide (DMSO), and acetonitrile (ACN) have been studied by density functional theory calculations together with ab initio molecular dynamics simulations. The calculated diffusivities of Li^+ and LiO_2 in all three solvent are rather low and follow the trend of the solvation energies of these species. Their transformation together with oxygen reduction are crucial reactions occuring in Li-air batteries. Our simulations using the Blue moon ensemble confirm experimental findings that upon the interaction of Li^+

with O_2^- first LiO_2 is formed which then further disproportionates to Li_2O_2. These reactions occur spontaneously in all three considered organic solvents, but the energy gain is reduced compared to the gas phase, in particular due to the higher stabilization of the ionic educts with regard to the molecular products in the electrolyte. This study represents a first step towards a more complete first-principles based understanding of the crucial processes occurring in the electrolytes of Li-air batteries which is needed to overcome obstacles in their reversible operation.

Acknowledgements

This research has been supported by the German Research Foundation (DFG) through contract GR 1503/38-1. The authors acknowledge the computer time supplied by the state of Baden-Württemberg through the bwHPC project and the Germany Research Foundation (DFG) through grant number INST 40/467-1 FUGG (JUSTUS cluster). This work contributes to the research performed at CELEST (Center for Electrochemical Energy Storage Ulm-Karlsruhe).

References

[1] J. Christensen, P. Albertus, R. S. Sanchez-Carrera, T. Lohmann, B. Kozinsky, R. Liedtke, J. Ahmed, A. Kojic, A critical review of Li/Air batteries, J. Electrochem. Soc. 159 (2011) R1–R30. doi:10.1149/2.086202jes.

[2] P. G. Bruce, S. A. Freunberger, L. J. Hardwick, J.-M. Tarascon, Li–O_2 and Li–S batteries with high energy storage, Nat. Mat. 11 (2012) 19–29. doi:10.1038/NMAT3191.

[3] D. Aurbach, B. D. McCloskey, L. F. Nazar, P. Bruce, Advances in understanding mechanisms underpinning lithium–air batteries, Nat. Energy 1. doi:10.1038/NENERGY.2016.128.

[4] H.-D. Lim, B. Lee, Y. Bae, H. Park, Y. Ko, H. Kim, J. Kim, K. Kang, Reaction chemistry in rechargeable Li–O_2 batteries, Chem. Soc. Rev. 46 (2017) 2873–2888. doi:10.1039/C6CS00929H.

[5] Y.-C. Lu, B. M. Gallant, D. G. Kwabi, J. R. Harding, R. R. Mitchell, M. S. Whittingham, Y. Shao-Horn, Lithium–oxygen batteries: Bridging mechanistic understanding and battery performance., Energy Environ. Sci. 6 (2013) 750–768. doi:10.1039/C3EE23966G.

[6] G. Girishkumar, B. McCloskey, A. C. Luntz, S. Swanson, W. Wilcke, ithium-air battery: Promise and challenges, J. Phys. Chem. Lett. 1 (14) (2010) 2193–2203. doi:10.1021/jz1005384.

[7] Z. Peng, S. A. Freunberger, L. J. Hardwick, Y. Chen, V. Giordani, F. Bardé, P. Novák, D. Graham, J.-M. Tarascon, P. G. Bruce, Oxygen reactions in non-aqueous Li^+ electrolytes, Angew. Chem. Int. Ed. 50 (2011) 6351 –6355. doi:10.1002/anie.201100879.

[8] S. Sakong, D. Mahlberg, T. Roman, M. Pandey, A. Groß, Influence of local inhomogenities and the electrochemical environment on the oxygen reduction reaction on Pt-based electrodes: A DFT study, J. Phys. Chem. C 124 (2020) 27604–27613. doi:10.1021/acs.jpcc.0c09548.

[9] L. Johnson, C. Li, Z. Liu, Y. Chen, S. A. Freunberger, P. C. Ashok, B. B. Praveen, K. Dholakia, J.-M. Tarascon, P. G. Bruce, The role of LiO_2 solubility in O_2 reduction in aprotic solvents and its consequences for Li-O_2 batteries, Nat. Chem. 6 (2014) 1091–1099. doi:10.1038/nchem.2101.

[10] Y. Shao, S. Park, J. Xiao, J.-G. Zhang, Y. Wang, J. Liu, Electrocatalysts for nonaqueous lithium–air batteries: Status, challenges, and perspective, ACS Catal. 2 (5) (2012) 844–857. doi:10.1021/cs300036v.

[11] T. K. Zakharchenko, A. Y. Kozmenkova, Isaev, D. M. Itkis, E. A. Goodolin, Lithium peroxide crystal clusters as a natural growth feature of dis-

charge products in Li–O_2 cells, Beilstein J. Nanotechnol. 4 (2013) 758–762. doi:10.3762/bjnano.4.86.

[12] Z.-L. Wang, D. Xu, J.-J. Xu, X.-B. Zhang, Oxygen electrocatalysts in metal–air batteries: from aqueous to nonaqueous electrolytes, Chem. Soc. Rev. 43 (2014) 7746–7786. doi:10.1039/C3CS60248F.

[13] A. V. Sergeev, A. V. Chertovich, D. M. Itkis, A. Sen, A. Gross, A. R. Khokhlov, Electrode/electrolyte interface in the Li–O_2 battery: Insight from molecular dynamics study, J. Phys. Chem. C 121 (2017) 14463–14469. doi:10.1021/acs.jpcc.7b03861.

[14] T. K. Zakharchenko, A. I. Belova, A. S. Frolov, O. O. Kapitanova, J.-J. Velasco-Velez, A. Knop-Gericke, D. Vyalikh, D. M. Itkis, L. V. Yashina, Notable reactivity of acetonitrile towards Li_2O_2/LiO_2 probed by NAP XPS during Li-O_2 battery discharge, Top. Catal. 61 (2018) 2114–2122. doi:10.1007/s11244-018-1072-5.

[15] T. K. Zakharchenko, A. Y. Kozmenkova, V. V. Isaev, D. M. Itkis, L. V. Yashina, Positive electrode passivation by side discharge products in Li–O_2 batteries, Langmuir 36 (2020) 8716–8722. doi:10.1021/acs.langmuir.0c00853.

[16] V. V. Isaev, A. V. Sergeev, T. K. Zakharchenko, D. M. Itkis, A. Groß, L. V. Yashina, Impact of cathodic electric double layer composition on the performance of aprotic Li-O_2 batteries, J. Electrochem. Soc. 168 (2021) 030520. doi:10.1149/1945-7111/abe6ec.

[17] B. R. Didar, L. Yashina, A. Groß, First-principles study of the surfaces and equilibrium shape of discharge products in Li-air batteries, ACS Appl. Mater. Interfaces 13 (2021) 24984–24994. doi:10.1021/acsami.1c05863.

[18] J. S. Hummelshøj, J. Blomqvist, S. Datta, T. Vegge, J. Rossmeisl, K. S. Thygesen, A. C. Luntz, K. W. Jacobsen, J. K. Norskøv, Communica-

tions: Elementary oxygen electrode reactions in the aprotic li-air battery, J. Chem. Phys. 132 (7) (2010) 1101–1104. doi:10.1063/1.3298994.

[19] M. D. Radin, J. F. Rodriguez, F. Tian, D. J. Siegel, Lithium peroxide surfaces are metallic, while lithium oxide surfaces are not, J. Am. Chem. Soc. 134 (2) (2012) 1093–1103. doi:10.1021/ja208944x.

[20] N. Seriani, Ab initio thermodynamics of lithium oxides: From bulk phases to nanoparticles, Nanotechnology 20 (44) (2009) 445703:1–7. doi:10.1088/0957-4484/20/44/445703.

[21] C. O. Laoire, S. Mukerjee, K. M. Abraham, E. J. Plichta, M. A. Hendrickson, Elucidating the mechanism of oxygen reduction for lithium-air battery applications, J. Phys. Chem. C 113 (46) (2009) 20127–20134. doi:10.1021/jp908090s.

[22] C. O. Laoire, S. Mukerjee, K. M. Abraham, E. J. Plichta, M. A. Hendrickson, Influence of nonaqueous solvents on the electrochemistry of oxygen in the rechargeable lithium-air battery, J. Phys. Chem. C 114 (2010) 9178–9186. doi:10.1021/jp102019y.

[23] D. G. Kwabi, V. S. Bryantsev, T. P. B. D. M. Itkis, C. V. Thompson, Y. Shao-Horn, Experimental and computational analysis of the solvent-dependent O_2/Li^+-$O_2{}^-$ redox couple, Angew.Chem. Int .Ed. 55 (2016) 3129 –3134. doi:10.1002/anie.201509143.

[24] F. S. Gittleson, R. E. Jones, D. K. Warda, M. E. Fostera, Oxygen solubility and transport in li–air battery electrolytes: Establishing criteria and strategies for electrolyte design, Energy Environ. Sci. 10 (2017) 1167–1179. doi:10.1039/C6EE02915A.

[25] Y. Wang, N.-C. Lai, Y.-R. Lu, Y. Zhou, C.-L. Dong, Y.-C. Lu, A solvent-controlled oxidation mechanism of Li_2O_2 in lithium-oxygen batteries, Joule 2 (11) (2018) 2364–2380. doi:10.1016/j.joule.2018.07.021.

[26] J. Xie, Q. Dong, I. Madden, X. Yao, Q. Cheng, P. Dornath, W. Fan, Achieving low overpotential Li-O_2 battery operations by Li_2O_2 decomposition through one-electron processes, Nano Lett. 15 (12) (2015) 8371–8376. doi:10.1021/acs.nanolett.5b04097.

[27] X. Lin, Z. Sun, C. Tang, Y. Hong, P. Xu, X. Cui, R. Y. Z. Zhou, M. Zheng, Q. Dong, Highly reversible O_2 conversions by coupling LiO_2 intermediate through a dual-site catalyst in Li-O_2 batteries, Adv. Energy Mater. 10 (2020) 001592(1–8). doi:10.1002/aenm.202001592.

[28] J. Scheers, D. Lidberg, K. Sodeyama, Z. Futera, Y. Tateyama, Life of superoxide in aprotic Li–O_2 battery electrolytes: Simulated solvent and counter-ion effects, Phys. Chem. Chem. Phys. 18 (2016) 9961–9968. doi:10.1039/C5CP08056H.

[29] A. Groß, Fundamental challenges for modeling electrochemical energy storage systems at the atomic scale, Top. Curr. Chem. 376 (2018) 17. doi:10.1007/s41061-018-0194-3.

[30] U. Das, K. C. Lau, P. C. Redfern, L. A. Curtiss, Structure and stability of lithium superoxide clusters and relevance to Li–O_2 batteries, J. Phys. Chem. Lett. 5 (5) (2014) 813–819. doi:10.1021/jz500084e.

[31] M. T. Ong, O. Verners, E. W. Draeger, A. C. T. van Duin, V. Lordi, J. E. Pask, Lithium ion solvation and diffusion in bulk organic electrolytes from first-principles and classical reactive molecular dynamics, J. Phys. Chem. B 119 (2015) 1535–1545. doi:10.1021/jp508184f.

[32] T. A. Pham, K. E. Kweon, A. Samanta, V. Lordi, J. E. Pask, Solvation and dynamics of sodium and potassium in ethylene carbonate from ab initio molecular dynamics simulations, J. Phys. Chem. C 121 (2017) 21913–21920. doi:10.1021/acs.jpcc.7b06457.

[33] M. I. Chaudhari, J. R. Nair, L. R. Pratt, F. A. Soto, P. B. Balbuena, S. B. Rempe, Scaling atomic partial charges of carbonate solvents for lithium

ion solvation and diffusion, J. Chem. Theory Comput. 12 (12) (2016) 5709–5718. doi:10.1021/acs.jctc.6b00824.

[34] V. S. Bryantsev, M. Blanco, F. Faglioni, Stability of lithium superoxide LiO_2 in the gas phase: Computational study of dimerization and disproportionation reactions, J. Phys. Chem. A 114 (31) (2010) 8165–8169. doi:10.1021/jp1047584.

[35] C. Xia, M. Waletzko, L. Chen, K. Peppler, P. J. Klar, J. Janek, Evolution of Li_2O_2 growth and its effect on kinetics of Li-O_2 batteries, ACS Appl. Mater. Interf. 6 (2014) 12083–12092. doi:10.1021/am5010943.

[36] Y. Zhang, X. Zhang, J. Wang, W. C. McKee, Y. Xu, Z. Peng, Potential-dependent generation of O_2- and LiO_2 and their critical roles in O_2 reduction to Li_2O_2 in aprotic Li-O_2 batteries, J. Phys. Chem. C 120 (2016) 3690–3698. doi:10.1021/acs.jpcc.5b12338.

[37] J. B. Haskins, H. H. Pham, A. Khetan, V. Viswanathan, J. W. Lawson, Lithium peroxide growth in Li-O_2 batteries via chemical disproportionation and electrochemical mechanisms: A potential-dependent ab initio study with implicit solvation, J. Phys. Chem. C 125 (2021) 436–445. doi:10.1021/acs.jpcc.0c08610.

[38] G. Kresse, J. Furthmüller, Efficient iterative schemes for ab initio total-energy calculations using a plane-wave basis set, Phys. Rev. B 54 (1996) 11169–11186. doi:10.1103/PhysRevB.54.11169.

[39] G. Kresse, D. Joubert, From ultrasoft pseudopotentials to the projector augmented-wave method, Phys. Rev. B 59 (1999) 1758–1775. doi:10.1103/PhysRevB.59.1758.

[40] P. E. Blöchl, Projector augmented-wave method, Phys. Rev. B 50 (1994) 17953–17979. doi:10.1103/PhysRevB.50.17953.

[41] J. P. Perdew, K. Burke, M. Ernzerhof, Generalized gradient approximation made simple, Phys. Rev. Lett. 77 (1996) 3865–3868.

doi:10.1103/PhysRevLett.77.3865.
URL https://link.aps.org/doi/10.1103/PhysRevLett.77.3865

[42] B. Hammer, L. B. Hansen, J. K. Nørskov, Improved adsorption energetics within density-functional theory using revised Perdew-Burke-Ernzerhof functionals, Phys. Rev. B 59 (1999) 7413–7421. doi:10.1103/PhysRevB.59.7413.

[43] S. Grimme, S. Ehrlich, L. Goerigk, Effect of the damping function in dispersion corrected density functional theory, J. Comput. Chem. 32 (2011) 1456–1465. doi:10.1002/jcc.21759.

[44] K. Forster-Tonigold, A. Groß, Dispersion corrected rpbe studies of liquid water, J. Chem. Phys. 141 (2014) 064501. doi:http://dx.doi.org/10.1063/1.4892400.

[45] S. Sakong, K. Forster-Tonigold, A. Groß, The structure of water at a Pt(111) electrode and the potential of zero charge studied from first principles, J. Chem. Phys. 144 (2016) 194701. doi:http://dx.doi.org/10.1063/1.4922615.

[46] D. Mahlberg, S. Sakong, K. Forster-Tonigold, A. Groß, Improved DFT adsorption energies with semiempirical dispersion corrections, J. Chem. Theory Comput. 15 (2019) 3250–3259. doi:10.1021/acs.jctc.9b00035.

[47] S. Nosé, A unified formulation of the constant temperature molecular-dynamics methods, J. Chem. Phys. 81 (1) (1984) 511–519. doi:10.1063/1.447334.

[48] W. G. Hoover, Canonical dynamics: Equilibrium phase-space distributions., Phys. Rev. A 31 (1985) 1695–1697. doi:10.1103/PhysRevA.31.1695.

[49] M. Dillenz, M. Sotoudeh, H. Euchner, A. Groß, Screening of charge carrier migration in the $MgSc_2Se_4$ spinel structure, Front. Energy Res. 8 (2020) 584654. doi:10.3389/fenrg.2020.584654.

[50] A. Einstein, The motion of elements suspended in static liquids as claimed in the molecular kinetic theory of heat, Ann. Phys. 17 (1905) 549–560.

[51] E. Carter, G. Ciccotti, J. T. Hynes, R. Kapral, Constrained reaction coordinate dynamics for the simulation of rare events, Chem. Phys. Lett. 156 (5) (1989) 472–477. doi:10.1016/S0009-2614(89)87314-2.

[52] M. Sprik, Free energy from constrained molecular dynamics, J. Chem. Phys. 109 (18) (1998) 7737–7744. doi:10.1063/1.477419.

[53] G. Ciccotti, M. Ferrario, Blue moon approach to rare events, Mol. Simul. 30 (11-12) (2004) 787–793. doi:10.1080/0892702042000270214.

[54] Y. Komeiji, Implementation of the blue moon ensemble method, Chem-Bio Inf. J. 7 (1) (2007) 12–23. doi:10.1273/cbij.7.12.

[55] P. Fleurat-Lessard, T. Ziegler, Tracing the minimum-energy path on the free-energy surface, J. Chem. Phys. 123 (2005) 084101(1)–(17). doi:10.1063/1.1948367.

[56] Y. Gohda, S. Schnur, A. Groß, Influence of water on elementary reaction steps in electrocatalysis, Faraday Discuss. 140 (2008) 233–244.

[57] S. Burlatsky, R. M. Darling, D. Novikov, V. V. Atrazhev, V. I. Sultanov, T. Y. Astakhova, L. Su, F. Brushett, Molecular dynamics modeling of the conductivity of lithiated nafion containing nonaqueous solvents, J. Electrochem. Soc. 163 (10) (2016) A2232–A2239. doi:10.1149/2.0461610jes.

[58] R. Semino, G. Zaldívar, E. J. Calvo, D. Laria, Lithium solvation in dimethyl sulfoxide-acetonitrile mixtures, J. Chem. Phys. 141 (2014) 214509. doi:10.1063/1.4902837.

[59] M. Sotoudeh, M. Dillenz, A. Groß, Mechanism of magnesium transport in spinel chalcogenides, Adv. Energy Sustainability Res. 2 (2021) 2100113. doi:10.1002/aesr.202100113.

[60] P. Ganesh, D.-E. Jiang, P. R. C. Kent, Accurate static and dynamic properties of liquid electrolytes for Li-ion batteries from ab initio molecular dynamics, J. Phys. Chem. B 115 (2011) 3085–3090. doi:10.1021/jp2003529.

[61] W. Yang, D. Y. Kim, L. Yang, N. Li, L. Tang, K. Amine, H.-K. Mao, Oxygen-rich lithium oxide phases formed at high pressure for potential lithium-air battery electrode, Adv. Sci. 4 (9) (2017) 1600453. doi:10.1002/advs.201600453.

[62] L. Johnson, C. Li, Z. Liu, Y. Chen, S. A. Freunberger, P. C. Ashok, B. B. Praveen, K. Dholakia, J.-M. Tarascon, P. G. Bruce, The role of LiO_2 solubility in O_2 reduction in aprotic solvents and its consequences for Li-O_2 batteries., Nat. Chem. 6 (2014) 1091–1099. doi:10.1038/nchem.2101.

[63] B. D. McCloskey, R. Scheffler, A. Speidel, G. Girishkumar, A. C. Luntz, On the mechanism of nonaqueous Li-O_2 electrochemistry on C and its kinetic overpotentials: Some implications for Li–air batteries, J. Phys. Chem. C 116 (45) (2012) 23897–23905. doi:10.1021/jp306680f.

[64] P. Albertus, G. Girishkumar, B. McCloskey, R. S. Sánchez-Carrera, B. Kozinsky, J. Christensen, A. C. Luntz, Identifying capacity limitations in the Li/oxygen battery using experiments and modeling, J. Electrochem. Soc. 158 (3) (2011) A343–A351. doi:10.1149/1.3527055.

[65] J. Huang, M. Li, M. J. Eslamibidgoli, M. Eikerling, A. Groß, Cation overcrowding effect on the oxygen evolution reaction, JACS Au 1 (2021) 1752–1765. doi:10.1021/jacsau.1c00315.